JACS
JOURNAL OF THE AMERICAN CHEMICAL SOCIETY
Article
pubs.acs.org/JACS

Compact Layer Free Perovskite Solar Cells with 13.5% Efficiency

Dianyi Liu,‡ Jinli Yang,‡ and Timothy L. Kelly*

Department of Chemistry, University of Saskatchewan, 110 Science Place, Saskatoon, Saskatchewan S7N 5C9, Canada

Supporting Information

ABSTRACT: The recent breakthrough of organometal halide perovskites as the light harvesting layer in photovoltaic devices has led to power conversion efficiencies of over 16%. To date, most perovskite solar cells have adopted a structure in which the perovskite light absorber is placed between carrier-selective electron- and hole-transport layers (ETLs and HTLs). Here we report a new type of compact layer free bilayer perovskite solar cell and conclusively demonstrate that the ETL is not a prerequisite for obtaining excellent device efficiencies. We obtained power conversion efficiencies of up to 11.6% and 13.5% when using poly(3-hexylthiophene) and 2,2′,7,7′-tetrakis(*N*,*N*-di(4-methoxyphenyl)amino)-9,9′-spirobifluorene, respectively, as the hole-transport material. This performance is very comparable to that obtained with the use of a ZnO ETL. Impedance spectroscopy suggests that while eliminating the ZnO leads to an increase in contact resistance, this is offset by a substantial decrease in surface recombination.

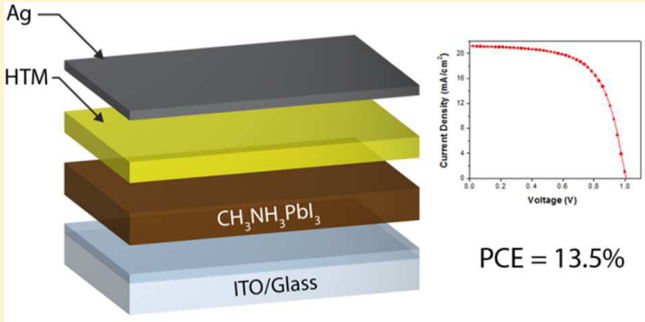

INTRODUCTION

The past four years have seen tremendous developments in the field of perovskite solar cells, with many researchers having been attracted by their low cost, simple fabrication, and high efficiency.[1−4] To date, both mesoscopic and planar perovskite solar cells have achieved 15−16% power conversion efficiencies (PCE),[5−12] with state-of-the-art mesoscopic devices having reached 17.9% certified PCE.[13] The high efficiencies arise from the combination of a high extinction coefficient, long charge-carrier diffusion lengths, and a relatively low bandgap.[14−18] These characteristics combine to produce devices with excellent short-circuit current densities (J_{sc}) and open-circuit voltages (V_{oc}); further, with qV_{oc}/E_g ratios over 0.7, the loss-in potentials of perovskite solar cells are substantially lower than those of either organic photovoltaic or dye-sensitized solar cells and have begun to approach those of GaAs-based devices.[19] This makes organolead halide perovskites some of the most promising new photovoltaic materials in decades.

The basis of any photovoltaic device is that the absorption of light produces charge carriers−electrons and holes. If the device is excitonic in nature, then free carriers must first be separated at a heterojunction whose energy level offsets are sufficient to overcome the exciton binding energy. However, even for materials with very weakly bound excitons, efficient device operation requires that electrons and holes be selectively and efficiently extracted at the anode and cathode. Therefore, substantial effort has gone into the development and study of interfaces for effective charge separation and carrier extraction. In probing the mechanism of operation of perovskite solar cells, Edri et al. found there are two key interfaces in perovskite solar cells, namely, the perovskite/electron-transport layer (ETL) interface and the perovskite/hole-transport layer (HTL) interface.[14] Their results indicated that the cell operates as a *p*−*i*−*n* device, with two essentially separate heterojunctions connected in series. Since the presence of both interfaces is not a prerequisite for device function, a number of reports have emerged on HTL-free perovskite solar cells;[20−25] these results clearly demonstrate that the devices can also perform well, even when the hole-selective contact is entirely absent. Etgar et al. have used $CH_3NH_3PbI_3$ and $CH_3NH_3PbBr_3$ light absorbers, in combination with a mesoscopic TiO_2 ETL, to deliver a maximum cell efficiency of 10.9% under AM1.5G irradiation.[23] Other groups have obtained PCEs of up to 10.5% using very similar device architectures.[24] Most notably, Mei et al. reported a HTL-free device based on a lead iodide perovskite containing a mixture of methylammonium and 5-aminovaleric acid cations.[25] A mesoporous ZrO_2 layer served to prevent recombination between the fully printable carbon electrode and the mesoporous TiO_2 ETL, resulting in a PCE of 12.8%. Yet despite these promising results, no analogous ETL-free devices have been reported in either regular or inverted architectures; so far, the ETL has been seen as a fundamental requirement for achieving PCEs > 10%.[1−4] Most high efficiency devices have used TiO_2 as the ETL, although ZnO nanoparticles[7] and fullerene-derivatives[26] have also been shown to work well.

These results are perhaps surprising, given our understanding of the mechanisms operative in a perovskite solar cell. Previous research has shown that the electron mobility in mesostructured $TiO_2/CH_3NH_3PbI_3$ films is lower than in either neat $CH_3NH_3PbI_3$ or in mesostructured $Al_2O_3/CH_3NH_3PbI_3$.[15,27]

Received: August 25, 2014
Published: November 18, 2014

   dx.doi.org/10.1021/ja508758k | J. Am. Chem. Soc. 2014, 136, 17116−17122

Therefore, from the perspective of electron transport, it may be more effective to eliminate the use of TiO_2, particularly in mesostructured form where the carrier-transport pathways are highly tortuous. Although previous reports have shown that incomplete surface coverage can result in the formation of pinholes when $CH_3NH_3PbI_3$ is deposited in a single step in the absence of a mesoporous scaffold,[28,29] a highly homogeneous film can be prepared by the two-step deposition method.[7] Additionally, the exciton binding energy in $CH_3NH_3PbI_3$ is estimated to be ∼50 meV,[30] meaning that >98% of the photogenerated excitons will thermally dissociate under normal operating temperatures. This suggests that the perovskite cell functions as a typical inorganic semiconductor thin-film device, where a high surface area heterojunction is not required for exciton separation. As such, it implies that the ETL should not be strictly necessary for high device performance.

In this work, we demonstrate a new compact layer free bilayer perovskite solar cell with a planar heterojunction structure. We compared the device performance of both perovskite and excitonic (bulk heterojunction) solar cells with and without a ZnO ETL and found that, while the ZnO layer was critical to the performance of the bulk heterojunction device, it could be entirely omitted in perovskite solar cells with very little drop in device performance. Analysis by electrochemical impedance spectroscopy (EIS) shows that the ZnO layer, while reducing the contact resistance at the ITO interface, also introduces additional surface recombination pathways. Therefore, the ZnO ETL can be completely eliminated with little impact on device performance. Additionally, the ZnO ETL is found to adversely impact device stability; as such, eliminating this superfluous layer results in both simpler device processing and improved device stability. The simpler fabrication process and increased thermal stability of the ZnO-free bilayer structure make these devices a very promising alternative to conventional perovskite cell designs.

EXPERIMENTAL SECTION

Solar Cell Fabrication. Solar cells were fabricated on precleaned ITO-coated glass substrates with a sheet resistance of 20 Ω/□. The cleaning procedure consisted of sequential ultrasonication for 30 min in dilute Extran 300 detergent, acetone, and isopropanol, followed by drying in an oven at 120 °C for 2 h. A PbI_2 solution (dissolved in *N*,*N*-dimethylformamide at a concentration of 460 mg/mL) was then spin coated onto the ITO surface at 3000 rpm for 15 s. After drying for several minutes in air, the substrate was dipped into a solution of CH_3NH_3I in 2-propanol (10 mg/mL) for 3 min, then dried under a flow of clean air. The HTL was then spin coated on top of the perovskite film. The P3HT-based HTL (20 mg of P3HT, 3.4 μL of 4-*tert*-butylpyridine, and 6.8 μL of a lithium-bis-(trifluoromethanesulfonyl)imide (Li-TFSI) solution (28 mg Li-TFSI/1 mL acetonitrile) all dissolved in 1 mL chlorobenzene) was deposited by spin coating at 1000 rpm for 30 s. The 2,2′,7,7′-tetrakis(*N*,*N*-di(4-methoxyphenyl)amino)-9,9′-spirobifluorene (Spiro-OMeTAD) HTL (80 mg of Spiro-OMeTAD, 28.5 μL of 4-*tert*-butylpyridine, and 17.5 μL of a Li-TFSI solution (520 mg Li-TFSI/1 mL acetonitrile) all dissolved in 1 mL chlorobenzene) was deposited by spin coating at 4000 rpm for 30 s. Finally, a 150 nm thick silver layer was deposited by thermal evaporation at a base pressure of 2×10^{-6} mbar. For the ETL-containing control devices, a thin ZnO nanoparticle layer[7,31] was first spin coated onto the ITO substrate at 3000 rpm for 30 s. This procedure was repeated three times. The PbI_2 solution was then spin coated on top of the ZnO layer at 3000 rpm for 15 s. All other procedures were the same as for the ZnO-free devices. Completed devices were stored in a N_2-purged glovebox (<0.1 ppm of O_2 and H_2O). Prior to the evaporation of the Ag top contact, all perovskite devices fabrication steps were carried out under ambient conditions. For polymer solar cells, a 10:8 solution of P3HT:$PC_{61}BM$ (15 mg/mL:12 mg/mL, respectively) was spin coated on an ITO- or ZnO-coated ITO substrate (20 Ω/□) at 1000 rpm for 30 s. After annealing at 150 °C for 10 min, a PEDOT:PSS (Clevios P VP AI 4083) layer was deposited by spin coating at 3000 rpm for 45 s and then annealing at 120 °C for 10 min. Finally, a 80 nm thick silver layer was deposited by thermal evaporation at a base pressure of 2×10^{-6} mbar.

Device Characterization. The current−voltage curves of solar cells were measured inside the glovebox using a Keithley 2400 source-measure unit. The cells were illuminated by a 450 W Class AAA solar simulator equipped with an AM1.5G filter (Sol3A, Oriel Instruments) at a calibrated intensity of 100 mW/cm^2, as determined by a standard silicon reference cell (91150V Oriel Instruments). The effective area of the cell was defined to be 0.071 cm^2 using a nonreflective metal mask. IPCE spectra were measured in air using a commercial IPCE setup (QE-PV-Si, Oriel Instruments). Monochromated light was chopped at a frequency of 30 Hz, and photocurrents were measured using a lock-in amplifier. Impedance spectroscopy measurements were carried out by Solartron SI1260 impedance/gain-phase analyzer, under dark and illumination conditions by applying a 5 mV voltage perturbation with the frequency ranging between 400 kHz and 0.1 Hz. SEM images were acquired on a Hitachi S-4800 field emission microscope. AFM measurements were carried out using a Dimension Hybrid (Bruker/Veeco Metrology) atomic force microscope operating in contact mode in air.

RESULTS AND DISCUSSION

Photovoltaic Performance with and without the ZnO Layer. The n-type metal oxides such as titanium oxide (TiO_x) and zinc oxide (ZnO) have been widely used in polymer solar cells[32,33] due to their transparency and high electron mobility. These same materials have also found ubiquitous use as the electron-transporting (hole-blocking) layer in perovskite solar cells;[1−4] even in devices that use a mesoporous (and insulating) Al_2O_3[27] or ZrO_2[34] scaffold, a compact TiO_2 blocking layer is typically first deposited on the transparent electrode. Since analogous devices lacking a HTL have already been fabricated and have been shown to perform well,[20−24] here we prepared planar heterojunction perovskite solar cells via a two-step deposition process[7,35] in two different architectures—both with and without a ZnO ETL (Figure 1)—in order to determine how the ETL influences cell performance. To compare these results to those of excitonic solar cells, we also fabricated and tested inverted bulk heterojunction cells based on poly(3-hexylthiophene) (P3HT)/[6,6]-phenyl-C_{61}-butyric acid methyl ester ($PC_{61}BM$) active layers in both the ITO/ZnO/P3HT:$PC_{61}BM$/PEDOT/Ag and ITO/P3HT:$PC_{61}BM$/PEDOT/Ag architectures.

The device architectures and an energy level diagram of the components are shown in Figure 1. ITO-coated float glass was either first coated with a layer of ZnO nanoparticles or used as-is; perovskite films were then deposited on top via the sequential deposition method.[7,35] Top-view and cross-sectional SEM images of the $CH_3NH_3PbI_3$ film are shown in Figure 1c, which highlight the relatively large crystallite size (ca. 150 nm) and excellent surface coverage produced by the two-step deposition technique. A P3HT layer was then spin coated on top of the perovskite as the hole-transport material, and a thermally evaporated silver film completed the device structure. The current−voltage (J−V) curves of the best devices are shown in Figure 2a. The best cell based on the ITO/ZnO/$CH_3NH_3PbI_3$/P3HT/Ag structure delivered a short-circuit current density of 18.8 mA/cm^2, a V_{oc} of 0.94 V, and a fill factor (FF) of 66.0%, leading to a PCE of 11.7% under standard

dx.doi.org/10.1021/ja508758k | J. Am. Chem. Soc. 2014, 136, 17116−17122

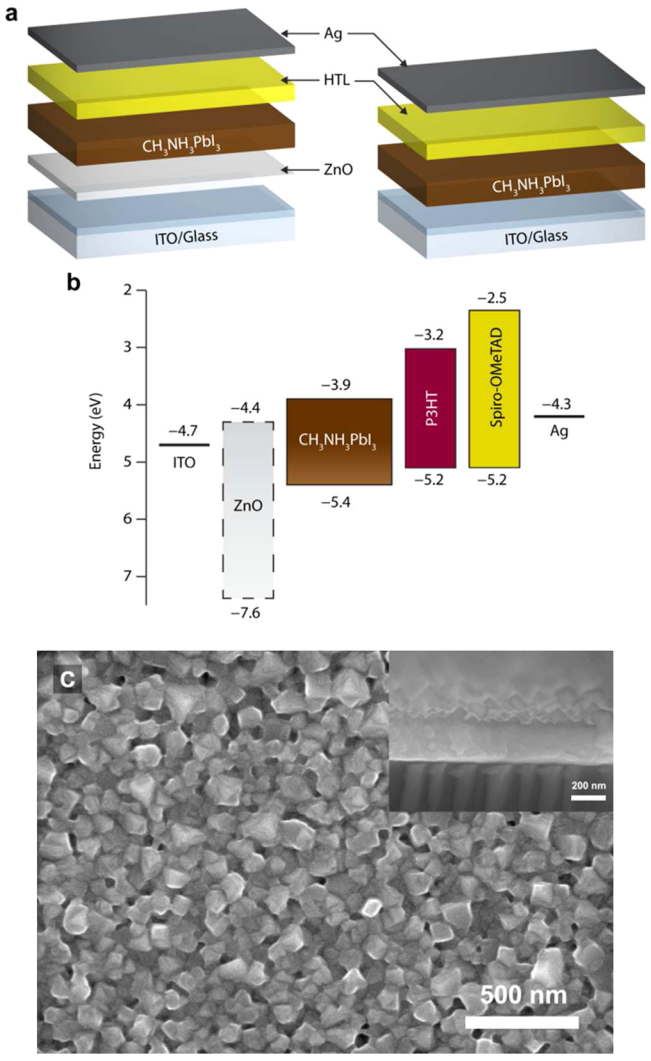

Figure 1. (a) Device architecture of the perovskite solar cells with and without a ZnO ETL; the HTL is either P3HT or Spiro-OMeTAD. (b) Energy levels of the individual device components. (c) SEM images of $CH_3NH_3PbI_3$ thin films on glass substrates: top-view (main) and cross-section (inset).

AM1.5G illumination. However, even without the ZnO ETL, the device performance is still highly competitive with this benchmark. The best ZnO-free device displayed a J_{sc} of 17.2 mA/cm^2, a V_{oc} of 1.01 V and a FF of 66.5%, which yielded a PCE of 11.6%. These numbers are in good agreement with the IPCE spectra. The onset of photocurrent at 800 nm is consistent with the optical bandgap of $CH_3NH_3PbI_3$,[36] and the IPCE spectrum effectively covers the entire visible region. The relatively flat spectral profile and high maximum efficiency (~75%) are indicative of excellent light harvesting efficiency. Integration of the product of the IPCE spectrum and the AM1.5G solar photon flux yields a projected current density of 17.1 mA/cm^2, which is in excellent agreement with the experimentally measured J_{sc}. Any differences between the simulated sunlight and the AM1.5G standard are therefore assumed to be negligible. The results were statistically validated by testing a batch of 76 separate ZnO-free devices. The average device performance parameters are summarized in Table S1, alongside those of ZnO-based control devices. The average J_{sc} and FF are very slightly lower for the ZnO-free devices than for the ZnO-based controls; however, this is offset by a slightly higher V_{oc}. The net result is that the overall power conversion efficiency of the ZnO-free devices is essentially indistinguishable from that of the cells prepared using a ZnO layer.

Additionally, since Spiro-OMeTAD has been shown to be a more effective hole-transport material than P3HT, we also fabricated ZnO-free devices using a Spiro-OMeTAD HTL. The ZnO-free $CH_3NH_3PbI_3$/Spiro-OMeTAD devices displayed PCEs of up to 13.5%, with an average value of 11.6% (Figure 2d). This compares very favorably with control devices containing a ZnO ETL, which were previously reported to have an average PCE of 13.7%.[7] It is worth noting that in both the P3HT and Spiro-OMeTAD devices, the V_{oc} is still ~1 V (Figure 2c). Clearly, the lack of a ETL does not result in extensive charge carrier recombination, which would be expected to substantially decrease the V_{oc}. In marked contrast, the polymer (P3HT:$PC_{61}BM$) solar cells show very different performance after removal of the ZnO layer (Figure 2b and Table S1). The highest performing ZnO-based control device had a J_{sc} of 9.81 mA/cm^2, a V_{oc} of 0.58 V, and a FF of 64.2%, yielding a PCE of 3.62%. After the ZnO layer was removed, the PCE of the best device was reduced to 1.29%, only one-third that of the corresponding control device. While the J_{sc} of 8.16 mA/cm^2 represents only a modest decrease from the maximum of 9.81 mA/cm^2, the V_{oc} of 0.40 V and FF of 39.6% were dramatically lower. Here the ZnO ETL is absolutely essential to proper device function; without it, charge recombination at the polymer/ITO interface leads to a significant decrease in both V_{oc} and FF.

Photoluminescence and Electrochemical Impedance Spectroscopy. While the collapse in the performance of the P3HT:$PC_{61}BM$ system upon removal of the ZnO ETL is to be expected, the anomalously high performance of the analogous ZnO-free perovskite cell is not. The substantial energy difference between the bottom of the perovskite conduction band and the ITO Fermi energy (0.8 eV) would ordinarily be expected to hinder efficient electron transfer across the perovskite/ITO interface; however, clearly that does not appear to be a limiting factor here. In order to better understand the high performance of the ZnO-free devices, photoluminescence spectroscopy was used to compare the relative efficiency of electron and hole extraction from the perovskite.

Figure 3 shows the photoluminescence spectrum of the $CH_3NH_3PbI_3$ film in a variety of bilayer configurations, including Glass/$CH_3NH_3PbI_3$, Glass/ITO/$CH_3NH_3PbI_3$, Glass/ZnO/$CH_3NH_3PbI_3$, Glass/$CH_3NH_3PbI_3$/P3HT, and Glass/$CH_3NH_3PbI_3$/Spiro-OMeTAD. The photoluminescence peak at 760 nm is entirely consistent with previous reports of emission from $CH_3NH_3PbI_3$,[37] and the spectral position of the emission is consistent among all of the samples. However, from the intensity of the peak, it can be seen that there is a substantial quenching effect when the perovskite is placed in contact with either ITO or the HTL/ETL materials. Emission from the perovskite was almost entirely quenched upon contact with the two hole-transport materials (P3HT and Spiro-OMeTAD); however, only ~40% photoluminescence quenching was observed when the perovskite was deposited on either ZnO or ITO. This is consistent with carrier extraction at the perovskite/HTL interface being more efficient than at the ZnO or ITO/perovskite interface; given the high surface area of the perovskite/HTL interface (R_{rms} = 65 nm, Figure S1), and the more planar ZnO and ITO surfaces (R_{rms} = 13 and 3 nm, respectively), this is likely at least partially driven by morphological differences. Highly efficient hole extraction at

dx.doi.org/10.1021/ja508758k | J. Am. Chem. Soc. 2014, 136, 17116−17122

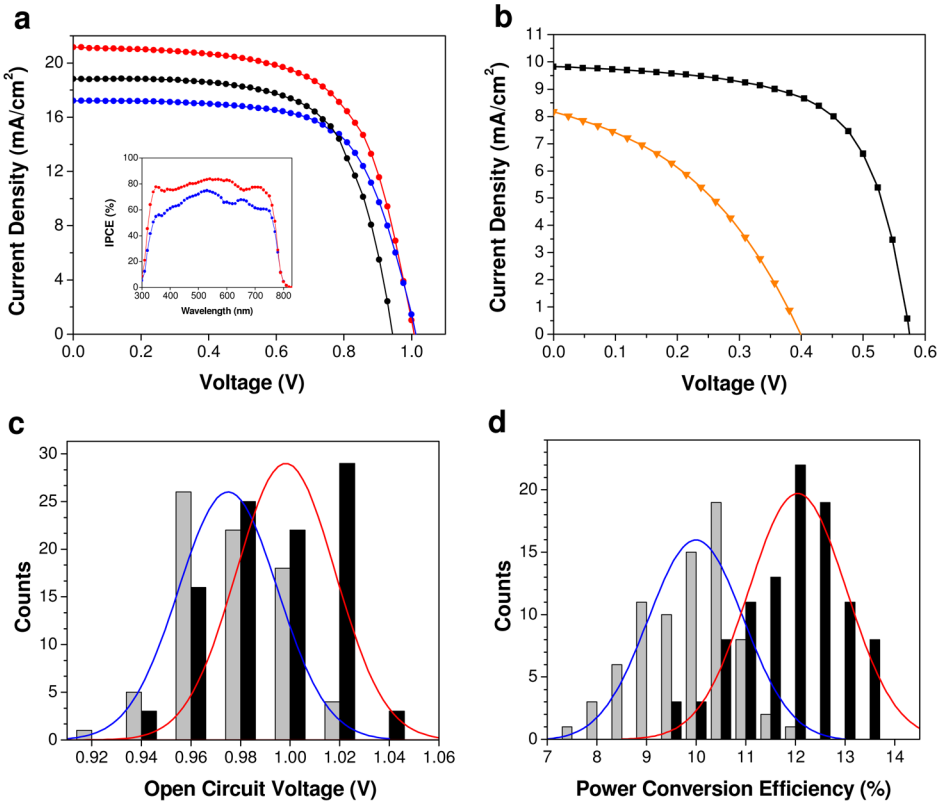

Figure 2. (a) $J-V$ curves of perovskite solar cells: P3HT HTL and ZnO ETL (black circles), P3HT HTL and no ETL (blue circles), Spiro-OMeTAD HTL and no ETL (red circles). The inset shows the IPCE spectra of the ZnO-free perovskite solar cells using P3HT (blue circles) and Spiro-OMeTAD (red circles) as the HTL. (b) $J-V$ curves of P3HT:$PC_{61}BM$ polymer solar cells both with (black squares) and without (orange triangles) a ZnO ETL. (c and d) Histograms of V_{oc} and PCE measured for 76 separate $CH_3NH_3PbI_3$/P3HT devices (gray) and 98 separate $CH_3NH_3PbI_3$/Spiro-OMeTAD (black) devices. The Gaussian fits are provided as a guide to the eye: $CH_3NH_3PbI_3$/P3HT (blue line), $CH_3NH_3PbI_3$/Spiro-OMeTAD (red line).

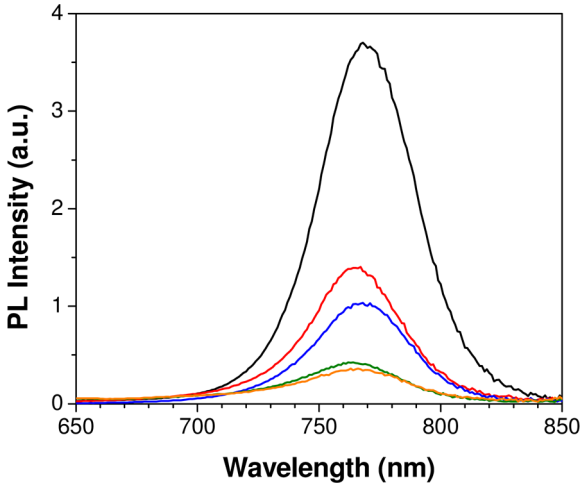

Figure 3. Photoluminescence spectra of perovskite films: Glass/$CH_3NH_3PbI_3$ (black line), Glass/ITO/$CH_3NH_3PbI_3$ (red line), Glass/ZnO/$CH_3NH_3PbI_3$ (blue line), Glass/$CH_3NH_3PbI_3$/P3HT (green line), and Glass/$CH_3NH_3PbI_3$/Spiro-OMeTAD (orange line).

the perovskite/HTL interface would at least partially explain the high performance of the ZnO-free devices; by rapidly depleting the perovskite of holes, bimolecular recombination would be at least partially suppressed. It is also important to note that the degree of photoluminescence quenching in the Glass/ZnO/$CH_3NH_3PbI_3$ and Glass/ITO/$CH_3NH_3PbI_3$ samples is very similar. Since the R_{rms} values of both the ZnO and ITO surfaces are not dramatically different (both form essentially flat interfaces with the perovskite) and both produce similar levels of photoluminescence quenching, it can be concluded that they have similar rates of electron transfer at the interface.

In order to better understand charge-transport and interfacial charge-transfer processes, we carried out EIS on both ITO/$CH_3NH_3PbI_3$/P3HT/Ag and ITO/ZnO/$CH_3NH_3PbI_3$/P3HT/Ag devices (Figure 4). EIS is a powerful characterization technique for studying the interfacial charge-transfer properties of photovoltaic devices[38] and has recently been used to investigate the carrier transport and recombination dynamics in mesostructured perovskite solar cells.[39−43] Figure 4a shows the Nyquist plots of devices both with and without ZnO ETLs, as measured at the open circuit potential under 1 sun AM1.5G illumination. Nyquist plots of the same devices in the dark are shown in Figure S2. The data in the Nyquist plot are clearly separated into two distinct *RC* arcs; although recent reports have occasionally revealed the presence of a third feature at low frequencies,[39,40] we see no evidence for it in the present case. As such, we have fit the data to a relatively simple equivalent circuit (Figure 4b) consisting of a parallel *RC* and *R-CPE* element connected in series, along with an additional contribution from series resistance (R_s). Although more elaborate models have been used to describe both perovskite and solid-state dye-sensitized solar cells in the past,[40−42] we have elected to use the simplest model capable of producing a

dx.doi.org/10.1021/ja508758k | J. Am. Chem. Soc. 2014, 136, 17116−17122

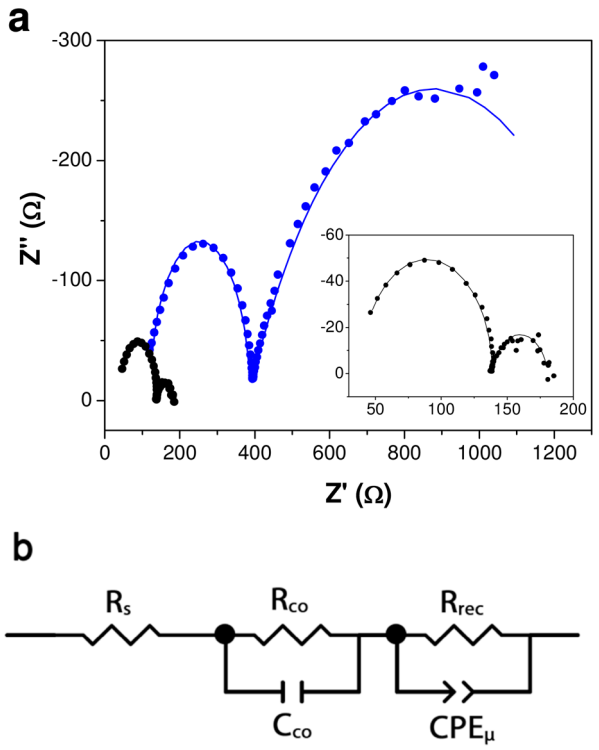

Figure 4. (a) Nyquist plots for the perovskite solar cells with (black circles) and without (blue circles) a ZnO ETL, as measured under 1 sun illumination at 0 V relative to the open circuit potential. The inset is an expanded view of the Nyquist plot for the cell containing a ZnO layer. Experimental data are shown as solid circles; the theoretical fits are shown as solid lines. (b) Equivalent circuit employed to fit the Nyquist plots.

good fit to the experimental data. The model is essentially identical to that used by Boix et al. in their analysis of solid-state Sb_2S_3 photovoltaic devices,[44] where the high-frequency *RC* element is ascribed to contact resistance at either the ETL/absorber or absorber/HTL interface, while the lower frequency element is associated with the recombination resistance (R_{rec}) and chemical capacitance (C_μ) of the system.[44,45] In comparing the Nyquist plots for the devices with and without the ZnO layer, it can be seen that both arcs have been substantially affected; as such, we ascribe the higher frequency feature to the contact impedance associated with the ITO/perovskite or ZnO/perovskite interface (since the perovskite/P3HT interface is identical in both cases).

The data were then fit to the equivalent circuit shown in Figure 4b, and the values of R_s, R_{co}, and R_{rec} are tabulated in Table S2. As expected, the devices that include a ZnO ETL have a reduced contact resistance, in keeping with the more favorable energy level alignment of the ZnO and perovskite conduction bands. This allows for more efficient extraction of the electrons at the ZnO/$CH_3NH_3PbI_3$ interface and is consistent with the slightly greater photoluminescence quenching observed for the Glass/ZnO/$CH_3NH_3PbI_3$ sample as opposed to the ITO analogue (Figure 3). However, from the perspective of overall device performance, this reduction in contact resistance is offset by a concomitant decrease in the recombination resistance. ZnO is known to provide high surface energy sites that can lead to substantial surface recombination; previous work has shown that high surface area ZnO nanostructures lead to relatively poor device performance, primarily due to losses in V_{oc} and FF attributed to surface recombination.[46] Our EIS data reinforce this idea and provide an explanation for the surprising performance of the ZnO-free devices: any losses that occur due to increased contact resistance and reduced electron extraction rates are simply offset by a reduction in surface recombination at the ZnO interface. The lack of surface recombination in the ZnO-free devices may also be due, in part, to residual unreacted PbI_2 that remains after the CH_3NH_3I dipping step. Previous work has suggested that a layer of PbI_2 adjacent to the transparent electrode may act as a built-in hole-blocking layer;[47] alternatively, since ITO itself is an n-type degenerate semiconductor, it may display some level of hole-blocking behavior.

By removing the ETL from the device architecture, we have been able to substantially simplify the device fabrication process; this is especially true considering that most electron-transport materials are deposited by spray pyrolysis or use similar high-temperature sintering steps. However, in removing the ETL, we also noticed an improvement in the stability of the devices. It is well-known that the $CH_3NH_3PbI_3$ light absorber is prone to decomposition in air;[48] however, this issue appears to be exacerbated when it is deposited on the ZnO ETL. We investigated the loss in device performance when the devices (using a P3HT HTL) were stored under ambient (relative humidity 30−40%; temperature 21−23 °C) conditions without any type of encapsulation. Though both sets of devices degraded very quickly under these conditions, the average degradation rate of the ZnO-free cells was slightly slower than that of the ZnO-based devices (Figure 5). Combined with the encouraging photovoltaic performance, these results suggest that ZnO-free devices are a promising alternative to conventional ETL/absorber/HTL architectures.

CONCLUSIONS

We have demonstrated for the first time compact layer free bilayer perovskite solar cells with performance comparable to that of devices that include a ZnO ETL. Photoluminescence and impedance spectroscopy measurements suggest that the origins of the high performance are two-fold: (i) highly efficient

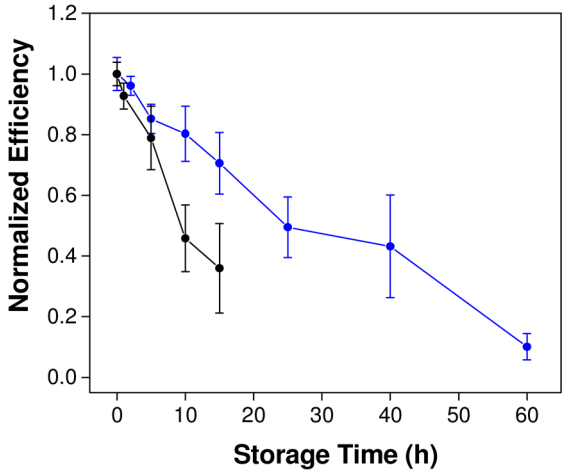

Figure 5. Normalized cell efficiency plotted as a function of storage time for perovskite solar cells both with (black circles) and without (blue circles) a ZnO ETL. Measurements were made on at least 24 devices of each type, and the error bars represent plus or minus one standard deviation from the mean.

dx.doi.org/10.1021/ja508758k | J. Am. Chem. Soc. 2014, 136, 17116−17122

hole extraction at the $CH_3NH_3PbI_3$/HTL interface results in a depletion of holes within the perovskite film, limiting opportunities for bimolecular recombination; and, (ii) reduced surface recombination at the ZnO-free interface offsets any losses due to the higher contact resistance. In a manner analogous to traditional inorganic thin-film solar cells, the low exciton binding energy and high charge carrier mobility of the perovskite light absorber are sufficient to produce efficient photovoltaic devices, even without two separate charge-selective layers. Compact layer free perovskite solar cells are a simple and effective photovoltaic technology that combines low costs with high efficiencies.

■ ASSOCIATED CONTENT

Supporting Information

Average photovoltaic device performance parameters, AFM images, Nyquist plots, and fitted EIS parameters. This material is available free of charge via the Internet at http://pubs.acs.org.

■ AUTHOR INFORMATION

Corresponding Author

tim.kelly@usask.ca

Author Contributions

‡These authors contributed equally.

Notes

The authors declare no competing financial interest.

■ ACKNOWLEDGMENTS

The Natural Sciences and Engineering Research Council of Canada (NSERC) and the University of Saskatchewan are acknowledged for financial support. T.L.K. is a Canada Research Chair in Photovoltaics. The research was undertaken, in part, thanks to funding from the Canada Research Chair program. Dr. Ian Burgess and Dr. Matthew Paige are gratefully acknowledged for their assistance with the EIS measurements and AFM image collection, respectively. Mr. Weihai Sun is gratefully acknowledged for SEM image collection.

■ REFERENCES

(1) Green, M. A.; Ho-Baillie, A.; Snaith, H. J. *Nat. Photonics* **2014**, *8*, 506.

(2) Gao, P.; Gratzel, M.; Nazeeruddin, M. K. *Energy Environ. Sci.* **2014**, *7*, 2448.

(3) Kazim, S.; Nazeeruddin, M. K.; Grätzel, M.; Ahmad, S. *Angew. Chem., Int. Ed.* **2014**, *53*, 2812.

(4) Snaith, H. J. *J. Phys. Chem. Lett.* **2013**, *4*, 3623.

(5) Burschka, J.; Pellet, N.; Moon, S.-J.; Humphry-Baker, R.; Gao, P.; Nazeeruddin, M. K.; Gratzel, M. *Nature* **2013**, *499*, 316.

(6) Liu, M.; Johnston, M. B.; Snaith, H. J. *Nature* **2013**, *501*, 395.

(7) Liu, D.; Kelly, T. L. *Nat. Photonics* **2014**, *8*, 133.

(8) Jeon, N. J.; Lee, H. G.; Kim, Y. C.; Seo, J.; Noh, J. H.; Lee, J.; Seok, S. I. *J. Am. Chem. Soc.* **2014**, *136*, 7837.

(9) Lee, J.-W.; Seol, D.-J.; Cho, A.-N.; Park, N.-G. *Adv. Mater.* **2014**, *26*, 4991.

(10) Xiao, M.; Huang, F.; Huang, W.; Dkhissi, Y.; Zhu, Y.; Etheridge, J.; Gray-Weale, A.; Bach, U.; Cheng, Y.-B.; Spiccia, L. *Angew. Chem.* **2014**, *53*, 9898.

(11) Wu, C.-G.; Chiang, C.-H.; Tseng, Z.-L. *J. Mater. Chem. A* **2014**, *2*, 15897.

(12) Jeon, N. J.; Noh, J. H.; Kim, Y. C.; Yang, W. S.; Ryu, S.; Seok, S. I. *Nat. Mater.* **2014**, *13*, 897.

(13) Green, M. A.; Emery, K.; Hishikawa, Y.; Warta, W.; Dunlop, E. D. *Prog. Photovoltaics: Res. Appl.* **2014**, *22*, 701.

(14) Edri, E.; Kirmayer, S.; Mukhopadhyay, S.; Gartsman, K.; Hodes, G.; Cahen, D. *Nat. Commun.* **2014**, *5*, 3461.

(15) Ponseca, C. S.; Savenije, T. J.; Abdellah, M.; Zheng, K.; Yartsev, A.; Pascher, T.; Harlang, T.; Chabera, P.; Pullerits, T.; Stepanov, A.; Wolf, J.-P.; Sundström, V. *J. Am. Chem. Soc.* **2014**, *136*, 5189.

(16) Sum, T. C.; Mathews, N. *Energy Environ. Sci.* **2014**, *7*, 2518.

(17) Stranks, S. D.; Eperon, G. E.; Grancini, G.; Menelaou, C.; Alcocer, M. J. P.; Leijtens, T.; Herz, L. M.; Petrozza, A.; Snaith, H. J. *Science* **2013**, *342*, 341.

(18) Xing, G.; Mathews, N.; Sun, S.; Lim, S. S.; Lam, Y. M.; Grätzel, M.; Mhaisalkar, S.; Sum, T. C. *Science* **2013**, *342*, 344.

(19) Nayak, P. K.; Cahen, D. *Adv. Mater.* **2014**, *26*, 1622.

(20) Etgar, L.; Gao, P.; Xue, Z.; Peng, Q.; Chandiran, A. K.; Liu, B.; Nazeeruddin, M. K.; Grätzel, M. *J. Am. Chem. Soc.* **2012**, *134*, 17396.

(21) Laban, W. A.; Etgar, L. *Energy Environ. Sci.* **2013**, *6*, 3249.

(22) Shi, J.; Dong, J.; Lv, S.; Xu, Y.; Zhu, L.; Xiao, J.; Xu, X.; Wu, H.; Li, D.; Luo, Y.; Meng, Q. *Appl. Phys. Lett.* **2014**, *104*, 063901.

(23) Aharon, S.; Gamliel, S.; Cohen, B. E.; Etgar, L. *Phys. Chem. Chem. Phys.* **2014**, *16*, 10512.

(24) Shi, J.; Luo, Y.; Wei, H.; Luo, J.; Dong, J.; Lv, S.; Xiao, J.; Xu, Y.; Zhu, L.; Xu, X.; Wu, H.; Li, D.; Meng, Q. *ACS Appl. Mater. Interfaces* **2014**, *6*, 9711.

(25) Mei, A.; Li, X.; Liu, L.; Ku, Z.; Liu, T.; Rong, Y.; Xu, M.; Hu, M.; Chen, J.; Yang, Y.; Grätzel, M.; Han, H. *Science* **2014**, *345*, 295.

(26) Malinkiewicz, O.; Yella, A.; Lee, Y. H.; Espallargas, G. M.; Graetzel, M.; Nazeeruddin, M. K.; Bolink, H. J. *Nat. Photonics* **2014**, *8*, 128.

(27) Lee, M. M.; Teuscher, J.; Miyasaka, T.; Murakami, T. N.; Snaith, H. J. *Science* **2012**, *338*, 643.

(28) Eperon, G. E.; Burlakov, V. M.; Docampo, P.; Goriely, A.; Snaith, H. J. *Adv. Funct. Mater.* **2013**, *24*, 151.

(29) Jeng, J.-Y.; Chiang, Y.-F.; Lee, M.-H.; Peng, S.-R.; Guo, T.-F.; Chen, P.; Wen, T.-C. *Adv. Mater.* **2013**, *25*, 3727.

(30) D'Innocenzo, V.; Grancini, G.; Alcocer, M. J.; Kandada, A. R.; Stranks, S. D.; Lee, M. M.; Lanzani, G.; Snaith, H. J.; Petrozza, A. *Nat. Commun.* **2014**, *5*, 3586.

(31) Beek, W. J. E.; Wienk, M. M.; Kemerink, M.; Yang, X.; Janssen, R. A. J. *J. Phys. Chem. B* **2005**, *109*, 9505.

(32) Chen, L.-M.; Xu, Z.; Hong, Z.; Yang, Y. *J. Mater. Chem.* **2010**, *20*, 2575.

(33) Sun, Y.; Seo, J. H.; Takacs, C. J.; Seifter, J.; Heeger, A. J. *Adv. Mater.* **2011**, *23*, 1679.

(34) Bi, D.; Moon, S.-J.; Haggman, L.; Boschloo, G.; Yang, L.; Johansson, E. M. J.; Nazeeruddin, M. K.; Gratzel, M.; Hagfeldt, A. *RSC Adv.* **2013**, *3*, 18762.

(35) Liang, K.; Mitzi, D. B.; Prikas, M. T. *Chem. Mater.* **1998**, *10*, 403.

(36) Baikie, T.; Fang, Y.; Kadro, J. M.; Schreyer, M.; Wei, F.; Mhaisalkar, S. G.; Graetzel, M.; White, T. J. *J. Mater. Chem. A* **2013**, *1*, 5628.

(37) Wehrenfennig, C.; Liu, M.; Snaith, H. J.; Johnston, M. B.; Herz, L. M. *J. Phys. Chem. Lett.* **2014**, *5*, 1300.

(38) Fabregat-Santiago, F.; Garcia-Belmonte, G.; Mora-Sero, I.; Bisquert, J. *Phys. Chem. Chem. Phys.* **2011**, *13*, 9083.

(39) Sanchez, R. S.; Gonzalez-Pedro, V.; Lee, J.-W.; Park, N.-G.; Kang, Y. S.; Mora-Sero, I.; Bisquert, J. *J. Phys. Chem. Lett.* **2014**, *5*, 2357.

(40) Kim, H.-S.; Mora-Sero, I.; Gonzalez-Pedro, V.; Fabregat-Santiago, F.; Juarez-Perez, E. J.; Park, N.-G.; Bisquert, J. *Nat. Commun.* **2013**, *4*, 2242.

(41) Dualeh, A.; Moehl, T.; Tetreault, N.; Teuscher, J.; Gao, P.; Nazeeruddin, M. K.; Gratzel, M. *ACS Nano* **2014**, *8*, 362.

(42) Gonzalez-Pedro, V.; Juarez-Perez, E. J.; Arsyad, W. S.; Barea, E. M.; Fabregat-Santiago, F.; Mora-Sero, I.; Bisquert, J. *Nano Lett.* **2014**, *14*, 888.

(43) Juarez-Perez, E. J.; Wuβler, M.; Fabregat-Santiago, F.; Lakus-Wollny, K.; Mankel, E.; Mayer, T.; Jaegermann, W.; Mora-Sero, I. *J. Phys. Chem. Lett.* **2014**, *5*, 680.

(44) Boix, P. P.; Lee, Y. H.; Fabregat-Santiago, F.; Im, S. H.; Mora-Sero, I.; Bisquert, J.; Seok, S. I. *ACS Nano* **2011**, *6*, 873.

(45) Mora-Seró, I.; Bisquert, J.; Fabregat-Santiago, F.; Garcia-Belmonte, G.; Zoppi, G.; Durose, K.; Proskuryakov, Y.; Oja, I.; Belaidi, A.; Dittrich, T.; Tena-Zaera, R.; Katty, A.; Lévy-Clément, C.; Barrioz, V.; Irvine, S. J. C. *Nano Lett.* **2006**, *6*, 640.
(46) Kumar, M. H.; Yantara, N.; Dharani, S.; Graetzel, M.; Mhaisalkar, S.; Boix, P. P.; Mathews, N. *Chem. Commun.* **2013**, *49*, 11089.
(47) Cao, D. H.; Stoumpos, C. C.; Malliakas, C. D.; Katz, M. J.; Farha, O. K.; Hupp, J. T.; Kanatzidis, M. G. *APL Mater.* **2014**, *2*, 091101.
(48) Stoumpos, C. C.; Malliakas, C. D.; Kanatzidis, M. G. *Inorg. Chem.* **2013**, *52*, 9019.
(49) Yu, H.; Wang, F.; Xie, F.; Li, W.; Chen, J.; Zhao, N. *Adv. Funct. Mater.* **2014**, DOI: 10.1002/adfm.201401872.